JOURNAL OF SOLID STATE CHEMISTRY **130,** 192–198 (1997)
ARTICLE NO. SC977279

The Structure of Yttrium Cobaltate from Neutron Diffraction

Apurva Mehta,*,[1] R. Berliner,† and Robert W. Smith‡

*Stanford Synchrotron Radiation Laboratory, Stanford Linear Accelerator Center, PO Box 4349, MS 69, Stanford, California 94309; †Research Reactor Center, University of Missouri, Columbia, Missouri 65211; and ‡Department of Physics, University of Nebraska at Omaha, Omaha, Nebraska 68182-0266

Received September 3, 1996; in revised form January 13, 1997; accepted January 14, 1997

The crystal structure of $YCoO_3$ has been determined from Rietveld analysis of the powder neutron diffraction data at 17, 100, and 300 K. At each temperature, the structure is a distorted perovskite with orthorhombic symmetry, space group *Pbnm* ($Z = 4$). The lattice parameters, at 300 K, are $5.1388(5) \times 5.4191(5) \times 7.3658(7)$ Å. Structural analysis indicates that the formal valence of cobalt in $YCoO_3$ is +3. Analysis of the Co–O distances and the absence of magnetic structure indicates that the majority of the Co^{3+} ions in $YCoO_3$ are in the low-spin (i.e. $t_{2g}^6 e_g^0$) state. The data also show that perhaps 10% of the Co^{3+} ions at 300 K (but insignificant fractions at 100 and 17 K) are in the high-spin state.

INTRODUCTION

Demazeau *et al.* (1) were the first to synthesize yttrium cobaltate, $YCoO_3$. They indexed the material on an orthorhombic cell and assumed that the structure was a distorted perovskite. Many rare earth cobaltates, including yttrium cobaltate, have been studied extensively for the past 2 decades because of their unusual electromagnetic properties. One of the unusual properties is that the magnetic susceptibility increases with temperature and then gradually decreases. $YCoO_3$, for example, has a broad susceptibility maximum at approximately 600 K (2, 3). It is commonly believed that the increase in magnetic susceptibility with temperature is associated with an electronic transition of the Co^{3+} ion from the low-spin (LS) state to the high-spin (HS) state (i.e., from $t_{2g}^6 e_g^0$ to $t_{2g}^4 e_g^2$.) To our knowledge, no attempt has yet been made to determine the crystal structure of $YCoO_3$ or the valence and spin state of cobalt below room temperature.

We report here the crystal structure of $YCoO_3$ at 17, 100, and 300 K, as well as the valence and spin state of cobalt, as determined from neutron diffraction measurements.

[1] To whom correspondence should be addressed.

EXPERIMENTAL PROCEDURES

Sample Synthesis

$YCoO_3$ was first prepared in a high-pressure apparatus (1). It was subsequently synthesized at ambient pressure in the presence of large basic cations such as potassium (3). We prepared $YCoO_3$ by decomposing an equimolar mixture of potassium nitrate (Johnson Matthey, 99.994%), yttrium oxalate nonahydrate (Johnson Matthey, 99.9%), and cobalt nitrate hexahydrate (Johnson Matthey, 99.5%). A well-ground mixture was decomposed at 600 K for 1 h, followed by a reaction for 40 h at 973 K, and a final reaction for 24 h at 1173 K. An analysis of the energy-dispersive X-ray spectrum of the 1173 K product indicated that the sample contained no potassium. We were, however, unable to synthesize $YCoO_3$ without potassium nitrate. Analysis of the X-ray powder diffraction pattern indicated that the 1173 K product, dark purple, almost black in color, was a primitive orthorhombic phase with a small amount (2–3%) of Y_2O_3. Since we began with a stoichiometric mixture of yttrium and cobalt, the primitive orthorhombic phase in the 1173 K synthesis was presumed to be yttrium-deficient $YCoO_3$. Longer reaction times at 1173 K and reactions at temperatures up to 1500 K did not significantly reduce the amount of Y_2O_3. Thornton *et al.* (3), in their synthesis from potassium cobalticyanide, were also unable to introduce a stoichiometric amount of yttrium in $YCoO_3$.

Diffraction Measurements

X-ray powder diffraction data were collected on a Rigaku automated diffractometer using Cu$K\alpha$ radiation in a horizontal θ–2θ Bragg–Bretano geometry. A preliminary scan was taken from 10°–60° 2θ with silicon (NIST SRM: 640b) as an internal standard. Equal amounts of silicon and the sample were ground under acetone, and the slurry was dried on a zero background quartz plate to form the diffraction mount. A list of the first 23 corrected peak positions was made (excluding the silicon peaks). Four of these peaks corresponded to Y_2O_3; the remaining peaks were indexed

0022-4596/97 $25.00

on an orthorhombic cell of dimensions $5.139(1) \times 5.418(1) \times 7.365(1)$ Å. Table 1 lists the 23 peaks and their indexing.

Neutron diffraction data were collected at the wavelength of 1.4873 Å on the PSD-II diffractometer at the University of Missouri Research Reactor (4). The finely ground sample was packed into a 3 mm quartz capillary, and the capillary was mounted in a displex closed cycle refrigerator. Neutron diffraction data from 5°–105° 2θ at an increment of 0.05° 2θ were collected at 17, 100, and 300 K. (Therefore, there were 2000 data points in each diffraction pattern.) The PSD-II diffractometer uses a linear position sensitive detector to collect data in 20° segments. A small error in placement of the detector for the subsequent segment or a small discrepancy in the counting rate between successive segments manifests itself as a discontinuous step in the background. Since the background is a rapidly decreasing function at low angles but is almost flat at high angles, the discontinuous step, if visible, is often visible only between segment one and two (i.e., at 24.8° 2θ). The 300 and 100 K data clearly show such steps; however, the transition from the first to the second segment is not as obvious in the 17 K data.

Analyses of the three sets of neutron diffraction data were performed via Rietveld full-profile analysis using the software package GSAS (5). (See below for the details of the structural analysis.) The background was modeled by a five-term Chebyshev polynomial. The Bragg peak profiles were modeled by a Simpson-rule integration of a six-term pseudo-Voigt shape function (three Guassian, two Lorentzian, and one peak asymmetry term) (6). Two theta zero offset was also refined. We used the neutron scattering lengths of 7.75, 2.49, and 5.80 fm for yttrium, cobalt, and oxygen, respectively. Atoms at each crystallographically distinct site were assigned separate isotropic displacement factors. The full-profile analysis was performed on an assemblage consisting of Y_2O_3 and $Y_{1-x}CoO_3$. Lattice parameters, atomic positions, and the displacement factors were refined for both phases. Vacancies on the yttrium and the oxygen sites in the $YCoO_3$ phase and the phase fraction of Y_2O_3 were also refined. Oxygen sites were found to be fully occupied. Their occupancy was not refined in the final refinements. The displacement factors for the yttrium ions for the 300 and 100 K refinements were found to be negative and the yttrium occupancy was found to vary from 17 to 300 K. We believe that the temperature of measurements is insufficient for any significant ionic diffusion and hence the concentration of vacancies on the yttrium site must remain invariant over the range of measurement. We, therefore, believe that the yttrium occupancy correlates to the yttrium displacement factor. We thus fixed the occupancy of the yttrium site in the 300 and 100 K refinements to the value refined at 17 K. By thus fixing the yttrium occupancy the yttrium displacement factors at 100 and 300 K were refined to positive values.

TABLE 1
A List of Peaks in the 300 K X-Ray Powder Diffraction Pattern

2θ	Rel. intensity (%)	Indexing[a]
20.578	0.54	Y_2O_3
21.104	1.32	1 0 1
23.899	2.14	1 1 0
24.189	2.16	0 0 2
26.818	19.25	1 1 1
29.217	4.94	Y_2O_3
33.081	22.06	0 2 0
34.951	100.00	1 1 2
35.302	11.16	0 2 1
38.808	0.88	2 1 0
39.541	0.59	1 2 1
40.768	7.16	2 1 1/1 0 3
41.386	3.43	0 2 2
42.939	7.31	2 0 2
43.601	0.44	Y_2O_3
44.171	8.15	1 1 3
45.141	1.95	1 2 2
46.235	1.74	2 1 2
48.585	2.88	Y_2O_3
48.853	28.52	2 2 0
49.485	12.39	0 0 4
50.141	6.36	0 2 3
50.494	11.08	2 2 1

[a] Peaks indexed on an orthorhombic cell of the dimensions $5.137(1) \times 5.418(1) \times 7.365(1)$ Å.

STRUCTURAL ANALYSIS

Determination of the Space Group Symmetry

From the list of the observed Bragg peaks (Table 1), the following extinction conditions for the $YCoO_3$ phase were inferred. No systematic absences were found for *hkl* or *hk*0 reflections. For *h*0*l*, only reflections with $h + l = \mathrm{E}$ (even) were observed. For 0*kl*, only reflections with $k = \mathrm{E}$ were observed. For *h*00, 0*k*0, and 00*l* reflections, *h*, *k*, and *l* were always even. From these systematic absences, the extinction symbol for $YCoO_3$ was determined to be P_{bn-} (see Table 3.2 of the International Tables for Crystallography (7)). The extinction symbol P_{bn-} implies that $YCoO_3$ crystallizes in either the space group *Pbnm* (special setting of *Pnam*) or the space group $Pbn2_1$ (special setting of $Pna2_1$).

Distorted Perovskite Structure

The intensity distribution of $YCoO_3$ is very similar to that of the rare earth orthoferrites, such as $GdFeO_3$ and $YFeO_3$. We constructed the starting structure for full-profile Rietveld refinement of $YCoO_3$ based on the structure of rare earth orthoferrites reported by Geller and Wood (8). Rare earth orthoferrites crystallize in a distorted perovskite-type structure. Geller and Wood solved these structures in space group *Pbnm* (8).

Following Geller and Wood, we constructed the *Pbnm* structure of $YCoO_3$ by putting yttrium atoms in the 4(*c*) site at ($x \approx 0.98$, $y \approx 0.06$, $\frac{1}{4}$), cobalt atoms in the 4(*b*) site at ($\frac{1}{2}$, 0, 0), and oxygen atoms in the 4(*c*) site at ($x \approx 0.05$, $y \approx 0.47$, $\frac{1}{4}$) and the 8(*d*) site at ($x \approx 0.71$, $y \approx 0.27$, $z \approx 0.05$). The oxygen atoms in 4(*c*) sites will be henceforth called the apical oxygens and labeled Oa; the oxygen atoms in the 8(*d*) sites will be called basal oxygens and labeled Ob.

Pbn2_1 is a proper subgroup of *Pbnm*. In space group *Pbn*2_1, there are no special Wyckoff sites and the general site has a multiplicity of 4. The loss of the mirror plane has the effect of breaking the symmetry operation relating the basal oxygens (i.e., the 8(*d*) site in *Pbnm*) at (x, y, z) and ($-x$, $-y$, $-z$). We therefore introduced an extra basal oxygen (Ob_2) at ($x \approx -0.71$, $y \approx -0.27$, $z \approx -0.05$). The combination of these two 4(*a*) sites produced the basal oxygen network formed by the 8(*d*) sites in the *Pbnm* structure. Multiplicity and positions of the other atoms, i.e., Y, Co, and Oa, were very similar to those in the *Pbnm* structure.

We refined the 300 K neutron diffraction data in *Pbnm* and *Pbn*2_1 structural symmetry. The results of the refinement are shown in Tables 2 and 3, respectively. The fit of the data in *Pbn*2_1 structural symmetry is marginally better. However, the *Pbn*2_1 structure has nine additional fitting parameters and the statistical analysis of the improvement of the fit based on a test such as Hamilton's R test (9) indicates that there is an 81.7% probability that the improvement in the fit is statistically insignificant. Further, the displacement factor for Ob_2 refines to an unrealistic (negative) value. (Notice that the average displacement factor for the two basal oxygens in *Pbn*2_1 symmetry, 0.65, is very similar to the displacement factor for the basal oxygen in *Pbnm* symmetry.) We therefore believe that the *Pbn*2_1 symmetry is an inappropriate representation of the structure of $YCoO_3$. We report only the *Pbnm* structural refinement for the 100 and 17 K data. Tables 4 and 5 list the results of these

TABLE 3
300 K Structural Parameters for $YCoO_3$ in the *Pbn*2_1 Symmetry

$R_{wp}(14) = 11.23\%$ $R_{F^2}(14) = 9.40\%$[b]
Wt. fraction of $Y_2O_3 = 3.2(2)\%$[a]

$YCoO_3$ $a = 5.1387(5)$ Å $b = 5.4190(5)$ Å $c = 7.3656(7)$ Å $Z = 4$

			B (Å^2)	Occupancy
Y	0.9805(8)	0.0688(7)	0.243(3)	0.1(2)	0.94(2)
Co	0.495(9)	0.005(9)	0.000(5)	0.5(4)	1.00
Oa	0.4050(10)	0.9729(9)	0.239(3)	0.8(2)	1.00
Ob_1	0.685(3)	0.308(3)	0.039(3)	1.9(4)	1.00
Ob_2	−0.700(2)	−0.297(2)	−0.059(2)	−0.6(2)	1.00

[a] Number in the parenthesis is the estimated standard deviation on the last significant digit(s).
[b] Calculation of R_{F^2} includes only the 140 $YCoO_3$ reflections.

TABLE 2
300 K Structural Parameters and Selected Bond Distances for $YCoO_3$ in *Pbnm* Symmetry

$R_{wp}(14) = 11.26\%$ $R_{F^2}(14) = 9.53\%$[b]
Wt. fraction of $Y_2O_3 = 3.2(1)\%$[a]

$YCoO_3$ $a = 5.1387(5)$ Å $b = 5.4190(6)$ Å $c = 7.3657(7)$ Å $Z = 4$

				B (Å^2)	Occupancy
Y	0.9807(7)	0.0686(7)	$\frac{1}{4}$	0.1(1)	0.98
Co	$\frac{1}{2}$	0	0	0.5(3)	1.00
Oa	0.4048(10)	0.9729(9)	$\frac{1}{4}$	0.7(2)	1.00
Ob	0.6937(7)	0.3013(7)	0.0491(4)	0.6(2)	1.00

	Multiplicity	Bond length (Å)
Co–Oa	2	1.911(2)
Co–Ob	2	1.947(4)
Co–Ob	2	1.940(4)
Y–Oa	1	2.240(5)
Y–Oa	1	2.267(5)
Y–Ob	2	2.258(5)
Y–Ob	2	2.440(5)
Y–Ob	2	2.558(4)

[a] Number in the parenthesis is the estimated standard deviation on the last significant digit(s).
[b] Calculation of R_{F^2} includes only the 140 $YCoO_3$ reflections.

TABLE 4
100 K Structural Parameters and Selected Bond Distances for $YCoO_3$ in *Pbnm* Symmetry

$R_{wp}(14) = 7.45\%$ $R_{F^2}(14) = 4.42\%$[b]
Wt. fraction of $Y_2O_3 = 3.0(4)\%$[a]

$YCoO_3$ $a = 5.1249(4)$ Å $b = 5.4153(4)$ Å $c = 7.3483(5)$ Å $Z = 4$

				B (Å^2)	Occupancy
Y	0.9816(4)	0.0695(4)	$\frac{1}{4}$	0.1(1)	0.98
Co	$\frac{1}{2}$	0	0	0.5(2)	1.00
Oa	0.4034(5)	0.9726(5)	$\frac{1}{4}$	0.3(1)	1.00
Ob	0.6931(4)	0.3016(4)	0.0488(2)	0.3(1)	1.00

	Multiplicity	Bond length (Å)
Co–Oa	2	1.908(1)
Co–Ob	2	1.943(2)
Co–Ob	2	1.938(2)
Y–Oa	1	2.225(3)
Y–Oa	1	2.261(3)
Y–Ob	2	2.257(3)
Y–Ob	2	2.439(3)
Y–Ob	2	2.546(2)

[a] Number in the parenthesis is the estimated standard deviation on the last significant digit(s).
[b] Calculation of R_{F^2} includes only the 140 $YCoO_3$ reflections.

TABLE 5
17 K Structural Parameters and Selected Bond Distances for $YCoO_3$ in *Pbnm* Symmetry

$R_{wp}(14) = 6.22\%$ $R_{F^2}(14) = 3.67\%$[b]
Wt. fraction of $Y_2O_3 = 2.0(1)\%$[a]

$YCoO_3$

	$a = 5.1232(4)$ Å	$b = 5.4139(4)$ Å	$c = 7.3457(5)$ Å	$Z = 4$
			B (Å^2)	Occupancy
Y	0.9818(3)	0.0693(3)	$\frac{1}{4}$	0.0(1)	0.98(1)
Co	$\frac{1}{2}$	0	0	0.3(1)	1.00
Oa	0.4025(4)	0.9740(4)	$\frac{1}{4}$	0.3(1)	1.00
Ob	0.6945(3)	0.3008(3)	0.0484(2)	0.3(1)	1.00

	Multiplicity	Bond length (Å)
Co–Oa	2	1.908(1)
Co–Ob	2	1.942(2)
Co–Ob	2	1.933(2)
Y–Oa	1	2.217(3)
Y–Oa	1	2.269(3)
Y–Ob	2	2.264(2)
Y–Ob	2	2.435(2)
Y–Ob	2	2.547(2)

[a] Number in the parenthesis is the estimated standard deviation on the last significant digit(s).
[b] Calculation of R_{F^2} includes only the 140 $YCoO_3$ reflections.

refinements. A few of the selected bond distances for the refined structures are also given in Tables 2, 4, and 5. Figure 1 shows a sketch of the *Pbnm* structure of yttrium cobaltate, and Figs. 2, 3, and 4 show the *Pbnm* structural fit to the 300, 100, and 17 K neutron data, respectively.

In an ideal (cubic) perovskite structure, the large A cation (i.e., yttrium in case of $YCoO_3$) is surrounded by 12 oxygens (i.e., by 4 Ob above, 4 Ob below, and 4 Oa in the equatorial plane), whereas the smaller B cation (i.e., cobalt in $YCoO_3$) is in oxygen octahedral coordination. The cobalt-centered octahedra in $YCoO_3$ are not ideal. The apical oxygens are a little closer to the cobalt than the basal oxygens. We believe that the small difference between the Co–Oa and Co–Ob bond distances is a manifestation of a Jahn–Teller distortion that breaks the degeneracy of the t_{2g} orbitals. However, the predominant deviation from the ideal perovskite symmetry in $YCoO_3$ arises from the rotation of the cobalt-centered octahedra. (The rotation can be designated as $a^-a^-c^+$ in Glazer's notation (10).)

The primary effect of the octahedral rotation in the *Pbnm* structure of $YCoO_3$ is to reduce the coordination of the Y^{3+} ion from 12 to 8 oxygens. Consequently, the yttrium is not coordinated in a standard close-packed 12-fold, i.e., cubic, symmetry, but is coordinated by 3 Ob from above, 3 Ob from below, and by only 2 Oa in the equatorial plane. In this configuration there are large openings in the equatorial region of the coordination sphere. These openings are

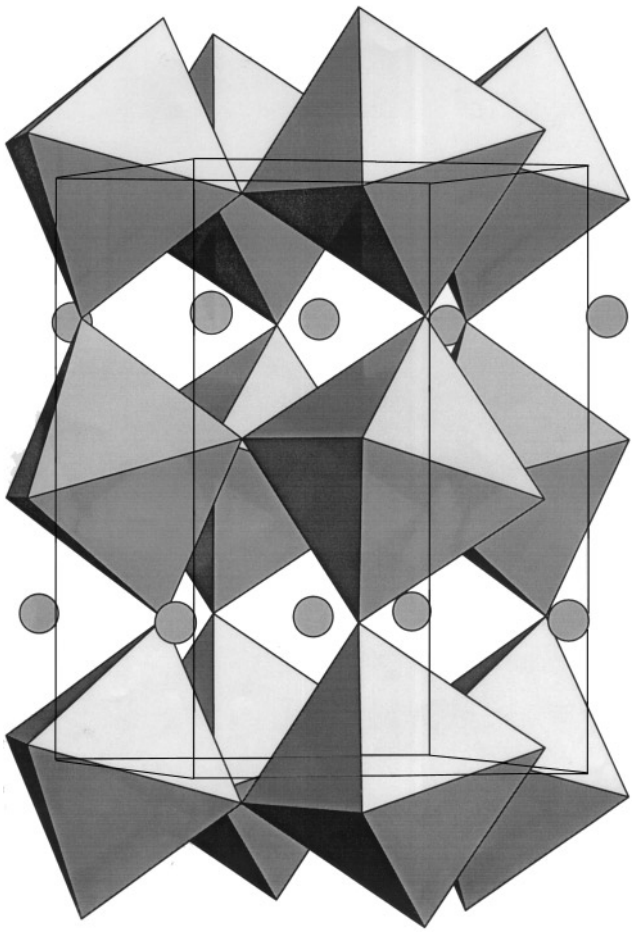

FIG. 1. A sketch of the *Pbnm* structure of $YCoO_3$ at 300 K. The unit cell boundaries are outlined. The a axis is horizontal, the b axis appears to go into the plane of the paper, and the c axis is vertical. The polyhedra represent the cobalt centered oxygen octahedra, and the gray spheres represent the yttrium ions.

filled by two distant oxygens (Oa), and even the nearest of these oxygens is more than 0.4 Å (at ≈ 3.0 Å) further away from the rest of the oxygens coordinating the yttrium ion. The effective close-packed coordination of yttrium is, therefore, perhaps 9 or 10 from these longer range oxygen interactions. Nevertheless, the Y^{3+} ion is too small to be fully coordinated by 12 oxygens as required in an ideal perovskite structure. We believe that the smaller coordinating requirement of the Y^{3+} ion is the primary driving force behind the deviation of $YCoO_3$ from the ideal perovskite structure.

The Goldschmidt-type tolerance factor (11), a measure of the stability of the perovskite structure, is 0.93 for $YCoO_3$. (For the calculation of the tolerance factor, we assumed yttrium to be in a 9-fold coordination. If yttrium were in 8-fold coordination, the tolerance factor would be 0.89.) The tolerance factor of 0.93 is just below the stability for the perovskite structure (12) and may explain the necessity of

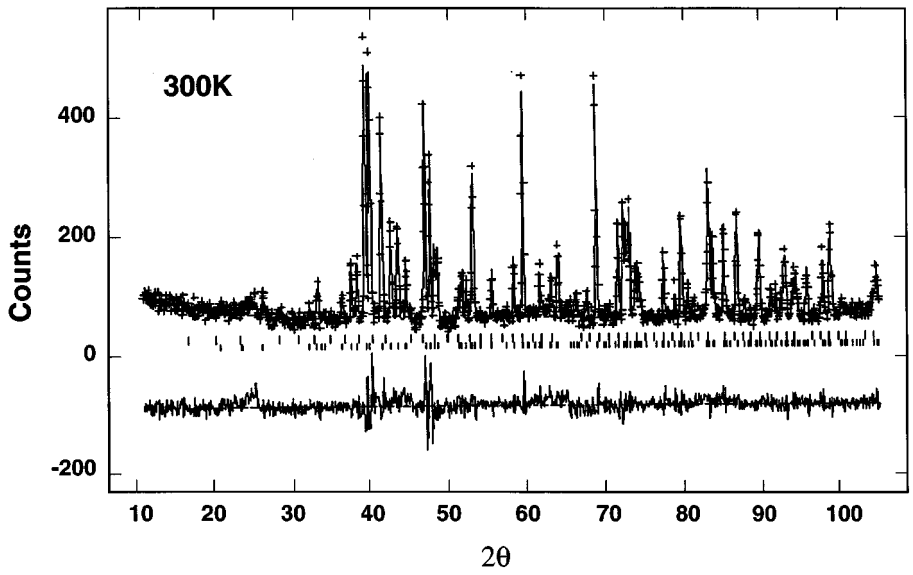

FIG. 2. The Rietveld refinement profile for the 300 K data, with $YCoO_3$ in *Pbnm* symmetry. The plus marks represent the experimental data, and the solid curve is the calculated profile. The difference between the two (experimental − calculated) is plotted at the bottom of the figure. The upper set of tick marks indicate the positions of Y_2O_3 reflections, and the bottom set indicates the positions of $YCoO_3$ reflections.

the highly oxidizing conditions required in its synthesis. Such synthesis conditions are created either by subjecting the reactants to high pressure or by including basic fluxes in the mixture of reactants. Replacement of the yttrium by one of the larger rare earth ions would increase the tolerance factor. The increased stability of the perovskite structure for the larger rare earth cobaltates is reflected in lower distortion from the ideal (cubic) symmetry, and the ease of synthesis, often without the aid of high pressures or basic fluxes.

Cobalt Valence and Spin State

Structural refinements indicate that both the oxygen sites in yttrium cobaltate are fully occupied within the error of

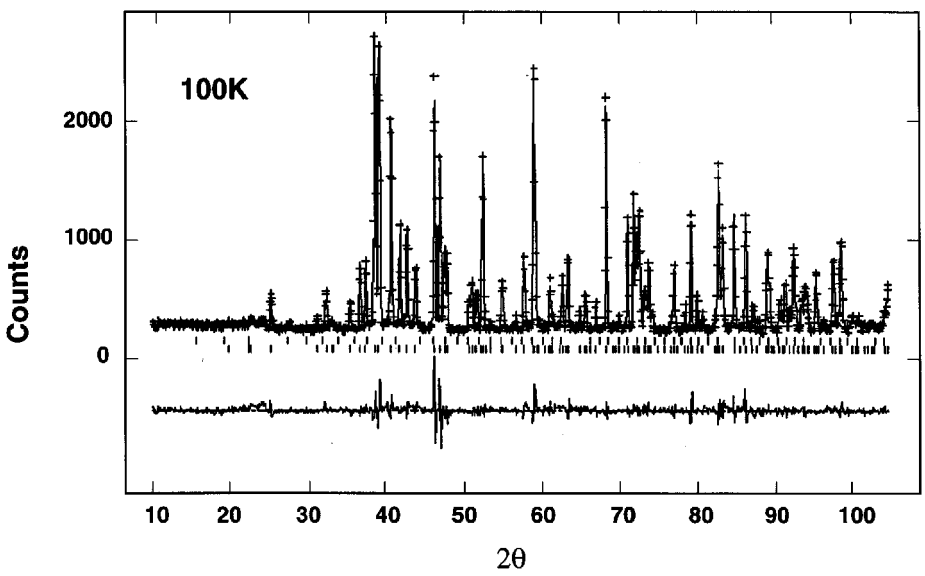

FIG. 3. The Rietveld refinement profile for the 100 K data, with $YCoO_3$ in *Pbnm* symmetry. The plus marks represent the experimental data, and the solid curve is the calculated profile. The difference between the two (experimental − calculated) is plotted at the bottom of the figure. The set of tick marks indicate the positions of Y_2O_3 reflections, and the bottom set indicates the positions of $YCoO_3$ reflections.

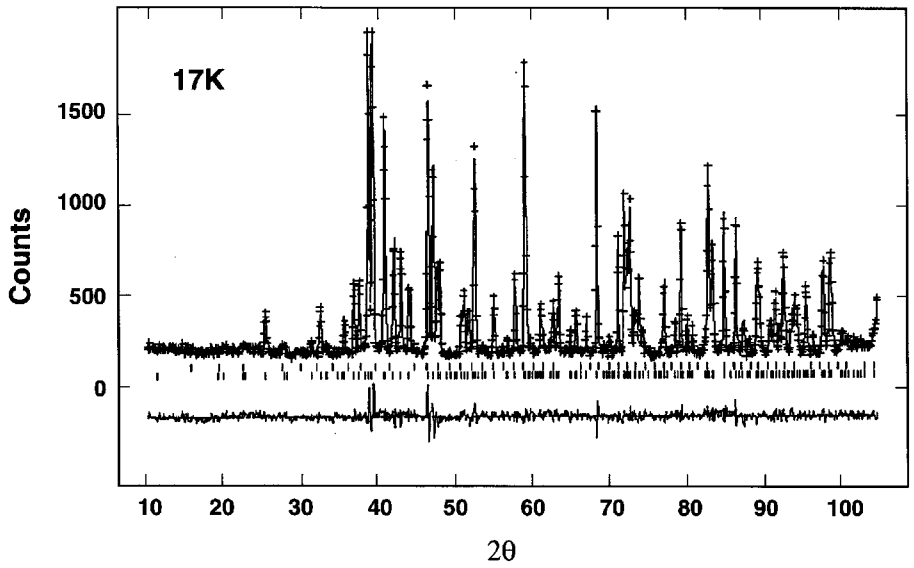

FIG. 4. The Rietveld refinement profile for the 17 K data, with $YCoO_3$ in *Pbnm* symmetry. The plus marks represent the experimental data, and the solid curve is the calculated profile. The difference between the two (experimental − calculated) is plotted at the bottom of the figure. The set of tick marks indicate the positions of Y_2O_3 reflections, and the bottom set indicates the positions of $YCoO_3$ reflections.

determination. The refinements, therefore, indicate that the formal valence of cobalt in $YCoO_3$ is + 3 (a little higher if the vacancy on the yttrium site is taken into consideration.)

The Co–O bond distances in $YCoO_3$ are 1.91–1.94 Å. These values compare well with the value of 1.925 Å from Shannon and Prewitt's (13) tabulation of 6-coordinated LS Co^{3+}–O distance. (Shannon and Prewitt assigned the oxide ion a radius of 1.40 Å for the determination of the cation radius.)

Co^{3+} has six 3*d* electrons. In an octahedral ligand field, the five 3*d* orbitals split into three lower energy t_{2g} orbitals and two higher energy e_g orbitals. In the LS state, pairing of electrons in the t_{2g} orbitals entails lower energy cost than promotion to the e_g orbitals. The six electrons of LS Co^{3+} in $YCoO_3$, therefore, occupy the three t_{2g} orbitals in pairs. As LS Co^{3+} has no unpaired electrons, it has no magnetic moment. Therefore, yttrium cobaltate appears to have no magnetic ions.

We could account for all the observed reflections in 17, 100, and 300 K neutron diffraction pattern by the nuclear structure of $YCoO_3$ and Y_2O_3 only. Hence, the neutron diffraction pattern of $YCoO_3$ from 17 to 300 K does not exhibit any purely magnetic reflections. Further, our attempts to refine a magnetic structure with reflections that coincided with the nuclear structure did not result in any significant improvement to the structural fit. The failure to obtain a reliable magnetic structure from the neutron diffraction data indicates that $YCoO_3$ has no discernible magnetic order from 17 to 300 K and supports our assertion that the bulk of the cobalt ions in this temperature range are in nonmagnetic LS states.

The structural fit to the 300 K neutron data, as measured by R_{F^2} (14), is poor in comparison with the fit of the lower temperature data (9.5% vs 4.4%; and 3.7%; see Tables 2, 4, and 5.) From analysis of difference Fourier synthesis maps and refinements of anisotropic displacement factors, it appears that the misfit to the 300 K data arises primarily from the modeling of the cobalt-centered octahedra. We found that the structural fit can be improved dramatically by replacing approximately 10% of the octahedra by expanded octahedra. The expansion is most significant in the Co–Ob bonds. The Co–O bond lengths, especially Co–Ob bond lengths, in the expanded octahedra are much too large for LS Co^{3+}–O, but are in keeping with the HS Co^{3+}–O distances reported by Shannon and Prewitt (13). Thus, the misfit to the 300 K $YCoO_3$ neutron data can be interpreted in terms of promotion of some of the LS Co^{3+} ($\approx$ 10%) to the HS state, although, as seen earlier, no long-range ordering of these spins is observed. From the quality of the structural fit to the 100 and 17 K data, and from the analysis of the difference Fourier maps generated from the fits, we conclude that insignificant amounts of Co^{3+} ions are in the HS state at these temperatures.

However, we caution that although the procedure of converting some of the LS cobalt-centered octahedra to HS significantly improves the structural fit to the 300 K data, the refinement suffers from severe correlations and instabilities. The instabilities suggest that the HS Co^{3+} ions may not inhabit the LS $YCoO_3$ randomly, but form a crystallographically distinct HS $YCoO_3$ phase. The refinement misfit at 300 K appears in the form of shoulders on some of the LS $YCoO_3$ peaks. The shoulder peaks are not very intense and

only a few of them are discernible, an observation consistent with the proposed HS $YCoO_3$ phase to be only a very small fraction of the sample at 300 K. Without an extensive set of allowed reflections we were unable to determine the space group symmetry of the HS $YCoO_3$ phase, and without the knowledge of the space group symmetry it is impossible to analyze the structure of a phase from powder diffraction data. Magnetic measurements on $YCoO_3$ indicate that the fraction of HS cobalt increases with temperature and thus, if HS cobalt ions form a new $YCoO_3$ phase, it will be more visible at higher temperatures. We, therefore, suggest high temperature structural investigations, especially in the vicinity of the susceptibility maximum at 600 K, to fully understand the character and arrangement of HS cobalt ions in $YCoO_3$.

ACKNOWLEDGMENTS

This work was supported by the Nebraska Research Initiative, the National Science Foundation under Grant OSR-9255225, and the Department of Energy under Grant DE-FG02-90ER45427.

REFERENCES

1. G. Demazeau, M. Pouchard, and P. Hagenmüller, *J. Solid State Chem.* **9,** 202 (1974).
2. see for instance, V. G. Jadhao, R. M. Singru, G. Rama Rao, D. Bahadur, and C. N. R. Rao, *J. Chem. Soc., Faraday Trans. 2*, **71,** 1885 (1975).
3. see for instance, G. Thornton, F. C. Morrison, S. Partington, B. C. Tofield, and D. E. Williams, *J. Phys. C: Solid State Phys.* **21,** 2871 (1988).
4. C. W. Thompson, D. F. R. Mildner, M. Mehregany, J. Sudol, R. Berliner, and W. B. Yelon, *J. Appl. Crystallogr.* **17**, 385 (1984); R. Berliner, K. McCollough, and J. Hilker-Draper, "A Position Sensitive Detector for Neutron Powder Diffraction," Final Technical Report, University Research Instrumentation Program, University of Missouri Research Agreement DAAL03-86-g-0150.
5. A. C. Larson and R. B. Von Dreele, Los Alamos National Laboratory Report, LAUR 86-748, 150, 1988.
6. C. J. Howard, *J. Appl. Crystallogr.* **15,** 615 (1982); P. Thompson, D. E. Cox, and J. B. Hastings, *J. Appl. Crystallogr.* **20,** 20 (1987).
7. "International Tables for Crystallography, Vol. A," Kluwer Academic, Dordrecht/Boston/London, 1989.
8. S. Geller and E. A. Wood, *Acta Crystallogr.* **9,** 563 (1956).
9. W. C. Hamilton, *Acta Crystallogr.* **18,** 502 (1965).
10. A. M. Glazer, *Acta Crystallogr., Sect. A* **31,** 756 (1975).
11. Tolerance factor $= (r_A + r_O)/\sqrt{2}(r_B + r_O)$. r_A, r_B, and r_O are the ionic radii of the large A cation, the smaller B cation (the cation in the oxygen octahedron), and the oxide ion, respectively.
12. A. Mehta, A. Navrotsky, N. Kumada, and N. Kinomura, *J. Solid State Chem.* **102,** 213 (1993).
13. R. D. Shannon and C. T. Prewitt, *Acta Crystallogr., Sect. B* **25,** 925 (1969).
14. $R_{wp} = \sqrt{\sum_i w_i (I_{io} - I_{ic})^2 / \sum_i w_i I_{io}^2}$ and $R_{F^2} = \sum_k F_{ko}^2 - F_{kc}^2 / \sum_k F_{ko}^2$; where I_{io} and I_{ic} are the observed and calculated intensities, w_i is the weight assigned to each data point, and F_{ko} and F_{kc} are the observed and the calculated structure factors.